

Localized kernel method for separation of linear chirps

S. Kitimoon*, E. Mason†, H. N. Mhaskar‡

July 4, 2025

Abstract

The task of separating a superposition of signals into its individual components is a common challenge encountered in various signal processing applications, especially in domains such as audio and radar signals. A previous paper by Chui and Mhaskar proposes a method called Signal Separation Operator (SSO) to find the instantaneous frequencies and amplitudes of such superpositions where both of these change continuously and slowly over time. In this paper, we amplify and modify this method in order to separate chirp signals in the presence of crossovers, a very low SNR, and discontinuities. We give a theoretical analysis of the behavior of SSO in the presence of noise to examine the relationship between the minimal separation, minimal amplitude, SNR, and sampling frequency. Our method is illustrated with a few examples, and numerical results are reported on a simulated dataset comprising 7 simulated signals.

Keywords: Chirp separation, signal separation operator

1 Introduction

The task of separating a superposition of signals into its individual components is a common challenge encountered in various signal processing applications, especially in domains such as audio [25, 28, 38] and radar [18, 11, 8, 3, 29, 23]. Due to the extensive set of applications and the frequent occurrence of signal source separation challenges, methodologies are often tailored to the specific field in question, as well as the level of prior knowledge of both the component signals and the mixing mechanism. We focus on a specific example that occurs in radar signal processing, specifically in the context of electronic warfare (EW) and electronic intelligence (ELINT).

In these applications, the RF system makes measurements of the electromagnetic spectrum with a large instantaneous bandwidth, typically above 1 GHz and continuing to increase with continual improvements in hardware capabilities. The resulting data may consist of tens to hundreds of signals mixed together after just a few seconds to minutes of recording, many overlapping in time and/or frequency and measured at low signal-to-noise (SNR). Most radars transmit a signal that consists of a sequence of linear frequency modulated (LFM) pulses, commonly referred to as Chirp signals.

A linear chirp is a signal (pulse) of the form $A(t) \exp(\hat{\mathbf{i}}\phi(t))$, where $\hat{\mathbf{i}} = \sqrt{-1}$ and ϕ is a quadratic polynomial, so that the instantaneous frequency $\phi'(t)$ is a linear function. If γ is the starting time of the pulse, d is its duration, θ is the initial frequency, B is the bandwidth, then the phase of the pulse is given by

$$\phi(t) = \phi(\gamma, \theta, B, d; t) = \theta(t - \gamma) + (B/d)(t - \gamma)^2. \quad (1.1)$$

The pulse is assumed to repeat periodically in m bursts with a pulse repetition interval PRI being the time between the end of one burst and the beginning of the next. Thus, for a signal s starting at $t = t_0^*$ its n -th burst is given by

$$s_n(t) = s_n(A, \theta, B, t_0^*, d, m, \text{PRI}; t) = \begin{cases} A(t) \exp\left(\hat{\mathbf{i}}(\theta(t - n * \text{PRI}) + (B/d)(t - n * \text{PRI})^2)\right), \\ \text{if } t_0^* + n * \text{PRI} \leq t \leq t_0^* + n * \text{PRI} + d, \quad n = 0, \dots, m - 1, \\ 0, & \text{otherwise.} \end{cases} \quad (1.2)$$

*Institute of Mathematical Sciences, Claremont Graduate University, Claremont, CA 91711, U.S.A..
email: sippanon.kitimoon@cgu.edu

†Hawkeye 360, Herndon, VA 20170, U.S.A. email: eric.mason@he360.com

‡Institute of Mathematical Sciences, Claremont Graduate University, Claremont, CA 91711, U.S.A.. The research of HNM was supported in part by ONR grants N00014-23-1-2394, N00014-23-1-2790. email: hrushikesh.mhaskar@cgu.edu

Naturally, the chirp signal has the form $s = \sum_n s_n$.

The first step in processing the electromagnetic spectrum is the detection and parameterization step, where the time and frequency locations of individual pulses are determined, and their parameters estimated. The second step in the EW receiver is deinterleaving, where groups of pulses are associated with each other to obtain the different radar signals, from which further insights are extracted. Here, we focus on the first problem of the detection, separation, and parameter estimation of individual radar pulses.

Thus, the problem which we intend to solve is the following. We observe a signal of the form

$$F(t) = f(t) + \epsilon(t), \quad (1.3)$$

where ϵ is a sub-Gaussian random noise, and f is the ground truth signal

$$f(t) = \sum_{j=1}^K s(A_j, \theta_j, B_j, t_{0,j}^*, d_j, m_j, \text{PRI}_j; t), \quad t \in [0, T]. \quad (1.4)$$

From equidistant observations $F(\ell\delta)$, $\ell = 0, \dots, N$, we wish to determine the number of pulses at any time t as well as the parameters $A_j, \theta_j, B_j, t_{0,j}^*, d_j, m_j, \text{PRI}_j$ of the pulses. In this paper, we will assume that all A_j 's are $\equiv 1$.

The instantaneous frequency of the chirp s_n in (1.2) at time t is defined by $\theta + (2B/d)(t - n * \text{PRI})$. Our approach is to assume (following [5, 4]) that on a sufficiently small interval of the form $[t - \Delta, t + \Delta]$, this frequency is approximated by a constant frequency at the center of the interval. We will then use specially constructed localized kernels to solve the problem for each of this interval as described in [26, 4]. A more elaborate subdivision is necessary when the instantaneous frequencies of different pulses cross each other. We will demonstrate experimentally that our method is very stable, capable of working with a very small SNR if the sampling rate is sufficiently high. Thus, the only limitation is the hardware capability, not a theoretical limitation. We will analyze theoretically the connection between Δ and the various parameters of the pulses and the accuracy.

The main contributions of this paper are the following.

1. This paper is the first of its kind that illustrates the use of SSO in the presence of a very high noise, crossover frequencies, and various components of the signal having different start and end points.
2. In particular, we describe how the SSO algorithm needs to be modified to detect the start and stop points of the various signal components and crossover frequencies.
3. We examine the theory behind the SSO to highlight the connection between the noise level, the sampling frequency, and the length of the snippet required for SSO to work properly.
4. Our algorithms are fully automated, assuming only the minimal separation among the instantaneous frequencies. The minimal separation can be treated as a tunable parameter, but its choice can affect the performance of the algorithm (cf. [27]).
5. Our algorithm works based on FFT, and hence, is very fast.

We will describe some related work in Section 2. The mathematical foundation behind our work is explained in Section 3, including the intuition and definition of the Signal Separation Operator (SSO) introduced in [4]. The algorithms and methodology to use SSO for the chirp separation problem are described in Section 4 with step-by-step illustrations on a few examples. In particular, the examples demonstrate the connection between the sampling rate, noise level, minimal separation among the instantaneous frequencies. A full report on the entire dataset which we worked on is presented in Section 5.

List of important symbols

Δ half-length of time interval for snippet

η minimal separation among frequencies

$\hat{\mathbf{i}}$ $\sqrt{-1}$

λ_j unitless, constant frequencies

$\Lambda_{j,k}$ estimated IF for chirp j at t_k

M Sum of absolute values of amplitudes
 $\mathcal{T}_{n,R}$ Signal separation operator
m minimal absolute value of amplitudes
 $\omega_{j,k}, \gamma_{j,k}, a_{j,k}$ Chirp parameters for chirp j in I_k
 Φ_n Localized trigonometric kernel
 σ_n Reconstruction operator
 τ threshold for SSO, estimate for $3\mathbf{m}/4$
 θ, γ, B, d Chirp parameters
 $A_j(t), \phi_j(t)$ Instantaneous complex amplitudes and phases
 B_{rec} Receiver bandwidth
 H low pass filter
 I_k time interval for snippet $[t_k - \Delta, t_k + \Delta]$
 R sampling frequency
 t_k center of the time interval for snippet
 V Variance parameter of a sub-Gaussian random variable
 PRI pulse repetition interval

2 Related works

There are several general ways to approach the problem of radar signal detection and separation.

In the case when the frequencies are constant, the problem is known as parameter estimation in exponential sums. This problem apparently goes back to the 1795 paper by Prony [7]. Mathematically, the problem can be stated as follows. Let $K \geq 1$ be an integer, $\{\lambda_j\}_{k=1}^K \subset (-\pi, \pi]$, $\mu = \sum_{j=1}^K A_j \delta_{\lambda_j}$ for some complex numbers $\{A_j\}_{k=1}^K$, where δ_x denotes the Dirac delta supported at x . Given noisy variants of the Fourier coefficients

$$\hat{\mu}(\ell) = \sum_{j=1}^K A_j \exp(-\hat{\mathbf{i}}\ell\lambda_j), \quad |\ell| < N, \quad (2.1)$$

for some integer $N \geq 1$ (where $\hat{\mathbf{i}} = \sqrt{-1}$), determine the locations λ_j and the coefficients A_j . Of course, finding λ_j 's is a bigger challenge; once we obtain these, the A_j 's can be found using a least square fit for the data (2.1). We will not go into a survey of the very large amount of literature on this problem, except to point out that our current work is based on ideas developed in [26, 4, 27].

If the radar pulses have sufficiently high SNR, then they can be detected using an energy-based envelope detector operating on the complex valued time-series data, known as In-phase and Quadrature (IQ) data [20, 19, 12]. It is actually more common for modern solid state radars to transmit low probability of intercept (LPI) waveforms that utilize LFM pulses at low and negative SNR [37, 30]; in this case, the envelope detector will no longer be suitable. In the low power setting, there are two broad classes of methods, the first operates on the IQ data directly, while the second utilizes time-frequency transforms approaching detection and separation as a 2D signal processing problem. In the time domain, there are analytic methods that operate on the IQ data directly, such as variations of independent components algorithm (ICA) [18, 22, 16, 33], with extensions to nonlinear chirps [32, 39], and incorporation of simple neural networks [31]. A more common approach is to utilize time-frequency transforms and process the result as an image instead of operating on the IQ data directly [17, 35, 2, 14, 24, 34].

A general framework that includes both the problems of chirp separation and parameter estimation in exponential sums is the following. One observes a signal of the form

$$f(t) = \sum_{j=1}^K f_j(t) = \sum_{j=1}^K A_j(t) \exp(\hat{\mathbf{i}}\phi_j(t)), \quad 0 \leq t \leq T, \quad (2.2)$$

where the instantaneous amplitudes (IA) A_j 's are complex valued, and ϕ_j 's are differentiable functions of time.

The quantity $\phi_j'(t)$ is known as the instantaneous frequency (IF) of the component f_j . The problem is to estimate the IFs and the IAs. This is also a very important and old problem, starting with a paper by a Nobel Laureate, Gabor [13]. One of the first approaches to solve the problem is the Hilbert-transform based empirical mode decomposition (EMD) by Huang [15]. However, there is no mathematical theory behind this approach. A mathematically rigorous approach was given by Daubechies and her collaborators [6, 5]. These seminal papers have given rise to a lot of variations and improvements. A complete survey is both beyond the scope of this paper as well as not relevant here. We refer to [21] for more references on this topic. In our paper, we will use the algorithm given in [36] for comparing our method with SST.

In [4], we have applied the technique based on localized trigonometric kernels to define a signal separation operator (SSO) to solve this problem under conditions weaker than those in [5]. Our conditions do assume that all the components are present in the interval $[0, T]$; i.e., the number of signals f_j is the same throughout the interval, and there is no discontinuity in any of these. Our method finds the IFs by looking at the peaks of a power spectrum rather than an elaborate reference curve mechanism of SST. Likewise, the IAs are estimated by a simple substitution compared to the limiting process required in SST. Finally, our method can be implemented very fast using FFT.

The paper [21] deals specifically with the separation of chirplets, based on a modification of a filter described in [4]. It is not clear when the various conditions in this paper are satisfied. Also, the method requires a three dimensional search. In this paper, we will demonstrate how the methods developed in [4] can be adapted for the chirp separation problem, including the case of crossover frequencies.

3 Mathematical foundations

In this section, we start in Section 3.1 by explaining the basic idea and theorem behind our methods in the case of signals with constant amplitudes and frequencies. In Section 3.2, we explain how the general problem of blind source signal separation can be reduced to this case at each point under certain assumptions as in [5, 4]. A theoretical analysis of the performance of SSO in the presence of noise is given in Section 3.3.

3.1 Constant amplitudes and frequencies

In the sequel, we write $\mathbb{T} = \mathbb{R}/(2\pi\mathbb{Z})$; i.e., \mathbb{T} is the quotient space of \mathbb{R} where x and y are identified if $x - y$ is an integer multiple of 2π . We describe first the case when the amplitudes and frequencies are constant; i.e., the problem of parameter estimation with the information of the form

$$\tilde{\mu}(\ell) = \sum_{j=1}^K A_j \exp(-\hat{\mathbf{i}}\ell\lambda_j) + \epsilon_\ell, \quad |\ell| < N, \quad (3.3)$$

where ϵ_ℓ 's are independent realizations of a sub-Gaussian random variable. This discussion summarizes the corresponding results in [27]. Following [1, Section 2.3], we recall that a real-valued random variable X is called sub-Gaussian with parameter V ($X \in \mathcal{G}(V)$) if $\mathbb{E}(X) = 0$ and $\log \mathbb{E}(\exp(tX)) \leq tV^2/2$ for all $t > 0$; e.g., if X is a mean zero normal random variable with variance V , then $X \in \mathcal{G}(V)$. Likewise, any bounded random variable is sub-Gaussian. We define a complex valued random variable X to be in $\mathcal{G}(V)$ if its real and imaginary parts are in $\mathcal{G}(V)$. It is not difficult to see that if X_1, \dots, X_n are i.i.d., complex valued variables all in $\mathcal{G}(V)$, $\mathbf{a} = (a_1, \dots, a_n) \in \mathbb{R}^n$, $|\mathbf{a}|_n^2 = \sum_{\ell=1}^n a_\ell^2$, then $\sum_{\ell=1}^n a_\ell X_\ell \in \mathcal{G}(|\mathbf{a}|_n V)$, and hence, that

$$\text{Prob} \left(\left| \sum_{\ell=1}^n a_\ell X_\ell \right| > t \right) \leq 4 \exp \left(-\frac{t^2}{4|\mathbf{a}|_n^2 V^2} \right), \quad t > 0. \quad (3.4)$$

A crucial role in our theory is played by certain localized trigonometric polynomial kernels, which we now define. Let $H : \mathbb{R} \rightarrow [0, 1]$ such that $H(t) = H(-t)$ for all $t \in \mathbb{R}$, $H(t)$ is a constant if $|t| \leq 1/2$, and $H(t) = 0$ if $|t| \geq 1$. The actual choice is not important for our theory, but we will take H to be fixed in the following discussion.

We define for

$$\hbar_n = \left\{ \sum_{|\ell| < n} H\left(\frac{|\ell|}{n}\right) \right\}^{-1}, \quad \Phi_n(x) = \hbar_n \sum_{|\ell| < n} H\left(\frac{|\ell|}{n}\right) e^{i\ell x}, \quad x \in \mathbb{T}, \quad n > 0. \quad (3.5)$$

We note that the normalizing factor \hbar_n is chosen so that

$$\max_{x \in \mathbb{T}} |\Phi_n(x)| = \Phi_n(0) = 1. \quad (3.6)$$

An important property of Φ_n is the following localization estimate: For every $S \geq 2$, there exists $L = L(H, S) \geq 1$ such that

$$|\Phi_n(x)| \leq \frac{L}{\max(1, (n|x|)^S)}, \quad x \in \mathbb{T}, \quad n > 0. \quad (3.7)$$

Explicit expressions for L in terms of H and S are given in [10]. The estimate (3.7) implies that $\Phi_n(x)$ is an approximation to the Dirac delta δ_0 .

The fundamental idea behind our approach is the following. We define

$$\sigma_n(\tilde{\mu})(x) = \hbar_n \sum_{|\ell| < n} H\left(\frac{|\ell|}{n}\right) \tilde{\mu}(\ell) e^{i\ell x}, \quad \sigma_n(\mu)(x) = \hbar_n \sum_{|\ell| < n} H\left(\frac{|\ell|}{n}\right) \hat{\mu}(\ell) e^{i\ell x}, \quad x \in \mathbb{T}. \quad (3.8)$$

Then it is not difficult to verify that

$$\sigma_n(\tilde{\mu})(x) = \sum_{j=1}^K A_j \Phi_n(x - \lambda_j) + E_n(x) = \sigma_n(\mu)(x) + E_n(x), \quad (3.9)$$

where

$$E_n(x) = \hbar_n \sum_{|\ell| < n} H\left(\frac{|\ell|}{n}\right) \epsilon(\ell) e^{i\ell x}, \quad x \in \mathbb{T}. \quad (3.10)$$

Because of the localization of Φ_n , one can deduce that $\sigma_n(\mu)(x)$ is small when x is away from each of the λ_j 's, and when it is large then x must be close to exactly one of the λ_j 's. Moreover, $E_n(x)$ being a weighted average of the noise realizations is small for large enough n . These observations are made precise in the following Theorem 3.1, proved in [27].

In this paper, we will encounter several constants whose values are hard to estimate, but not important to describe the results. We make the following convention.

Constant convention

The letters c, c_1, \dots will denote generic positive constants depending on H and S alone. Their values might be different at different occurrences, even within a single formula. The notation $A \lesssim B$ means $A \leq cB$, $A \gtrsim B$ means $B \lesssim A$, and $A \sim B$ means $A \lesssim B \lesssim A$. Constants denoted by capital letters, such as L, C , etc. will retain their values.

Before stating the main theorem, we estimate the noise term $E_n(x)$ in the following lemma [27, Lemma 4.1].

Lemma 3.1 *Let $\delta \in (0, 1)$. There exist positive constants C_1, C_2, C_3 , depending only on H such that for $n \geq C_1(\geq 1)$, we have*

$$\text{Prob} \left(\max_{x \in \mathbb{T}} |E_n(x)| \geq C_2 V \sqrt{\frac{\log(C_3 n / \delta)}{n}} \right) \leq \delta. \quad (3.11)$$

In order to state the main theorem of this section, we need some further notation. Let

$$\mathbf{M} = \sum_{j=1}^K |A_j|, \quad \mathbf{m} = \min_{1 \leq j \leq K} |A_j|, \quad \eta = \min_{\ell \neq k} |\lambda_j - \lambda_\ell|. \quad (3.12)$$

Our main theorem in this section can now be stated as follows.

Theorem 3.1 Let $0 < \delta < 1$,

$$\mathbb{G} = \{x \in [-\pi, \pi] : |\sigma_n(\tilde{\mu})(x)| \geq \mathbf{m}/2\}, \quad (3.13)$$

and (cf. (3.7), (3.12))

$$C = \left(\frac{16\mathbf{M}L}{\mathbf{m}} \right)^{1/S}. \quad (3.14)$$

Let n be large enough so that the estimate (3.11) holds, and in addition, $n \geq 4C/\eta$. Then each of the following statements holds with probability exceeding $1 - \delta$.

- **(Disjoint union condition)**
The set \mathbb{G} is a disjoint union of exactly K subsets \mathbb{G}_ℓ ,
- **(Diameter condition)**
For each $\ell = 1, \dots, K$, $\text{diam}(\mathbb{G}_\ell) \leq 2C/n$,
- **(Separation)**
 $\text{dist}(\mathbb{G}_\ell, \mathbb{G}_j) \geq \eta/2$ for $\ell \neq j$,
- **(Interval inclusion)**
For each $\ell = 1, \dots, K$, $I_\ell = \{x \in \mathbb{T} : |x - \lambda_\ell| \leq 1/(4n)\} \subseteq \mathbb{G}_\ell$.

Moreover, if

$$\hat{\lambda}_\ell = \arg \max_{x \in \mathbb{G}_\ell} |\sigma_n(x)|, \quad (3.15)$$

then

$$|\hat{\lambda}_\ell - \lambda_\ell| \leq 2C/n. \quad (3.16)$$

3.2 Reduction to the constant parameter case

In this section, we describe certain conditions under which the data of the form (2.2) can be reduced to the constant parameter data as in Section 3.1. Thus, we are interested finding the instantaneous frequencies $\phi'_j(t^*)$ and amplitudes $A_j(t^*)$ in the signal

$$f(t) = \sum_{j=1}^K f_j(t) = \sum_{j=1}^K A_j(t) \exp(\hat{\mathbf{i}}\phi_j(t)), \quad (3.17)$$

for some point $t^* \in \mathbb{R}$, where A_j 's are continuous and ϕ_j 's are continuously differentiable functions on an interval of the form $[t^* - \Delta, t^* + \Delta]$. We introduce the notation (abusing the notation introduced in (3.12))

$$\mathbf{M}(t^*) = \sum_{j=1}^K |A_j(t^*)|, \quad B(t^*) = \max_{1 \leq j \leq K} |\phi'_j(t^*)|. \quad (3.18)$$

The following theorem is a reformulation of [4, Theorem 4.2]. We will reproduce the proof for the sake of completeness.

Theorem 3.2 Let $t^* \in \mathbb{R}$, $\alpha, \Delta > 0$, and for $|u| \leq \Delta$,

$$|A_j(t^* + u) - A_j(t^*)| \leq \alpha|u||A_j(t^*)|, \quad |\phi'_j(t^* + u) - \phi'_j(t^*)| \leq \alpha|u||\phi'_j(t^*)|. \quad (3.19)$$

Then we have

$$\left| f(t^* + u) - \sum_{j=1}^K f_j(t^*) \exp(\hat{\mathbf{i}}\phi'_j(t^*)u) \right| \leq \alpha\mathbf{M}(t^*)(B(t^*)\Delta + 1)\Delta, \quad |u| \leq |\Delta|. \quad (3.20)$$

PROOF. In this proof, we write $\mathbf{M} = \mathbf{M}(t^*)$ and $B = B(t^*)$. Let $|u| \leq \Delta$. We observe that

$$\begin{aligned} & \left| \sum_{j=1}^K A_j(t^* + u) \exp(\hat{\mathbf{i}}\phi_j(t^* + u)) - \sum_{j=1}^K A_j(t^*) \exp(\hat{\mathbf{i}}\phi_j(t^*)) \exp(\hat{\mathbf{i}}u\phi'_j(t^*)) \right| \\ & \leq \left| \sum_{j=1}^K (A_j(t^* + u) - A_j(t^*)) \exp(\hat{\mathbf{i}}\phi_j(t^* + u)) \right| \\ & \quad + \left| \sum_{j=1}^K A_j(t^*) \left(\exp(\hat{\mathbf{i}}\phi_j(t^* + u)) - \exp(\hat{\mathbf{i}}\phi_j(t^*)) \exp(\hat{\mathbf{i}}u\phi'_j(t^*)) \right) \right| \end{aligned} \quad (3.21)$$

In view of the fact that

$$|e^{ix} - e^{iy}| = 2|\sin((x-y)/2)| \leq |x-y|,$$

and (3.19), we deduce that for each k ,

$$\begin{aligned} & \left| \exp(\hat{\mathbf{i}}\phi_j(t^* + u)) - \exp(\hat{\mathbf{i}}\phi_j(t^*)) \exp(\hat{\mathbf{i}}u\phi'_j(t^*)) \right| \leq |\phi_j(t^* + u) - \phi_j(t^*) - u\phi'_j(t^*)| \\ & \leq \left| \int_0^u (\phi'_j(t^* + v) - \phi'_j(t^*)) dv \right| \leq \alpha B \left| \int_0^u |v| dv \right| \leq \alpha B |u|^2 \leq \alpha B \Delta^2. \end{aligned} \quad (3.22)$$

Using (3.19) again, we see that

$$\left| \sum_{j=1}^K (A_j(t^* + u) - A_j(t^*)) \exp(\hat{\mathbf{i}}\phi_j(t^* + u)) \right| \leq \mathbf{M}\Delta.$$

Together with (3.22) and (3.21), this leads to (3.20). ■

3.3 Signal separation operator

In this section, we fix $t^* \in \mathbb{R}$. The quantities denoted below by α , Δ , R are independent of t^* , and so are the constants involved in \lesssim , \gtrsim , and \sim , but the other quantities will depend upon t^* without its mention in the notation.

Let $R > 0$ denote the sampling frequency. We write

$$\lambda_j = \phi'_j(t^*)/R, \quad n = \lfloor R\Delta \rfloor, \quad \mu = \sum_{j=1}^K f_j(t^*)\delta_{\lambda_j}, \quad \hat{\mu}(\ell) = \sum_{j=1}^K f_j(t^*) \exp(-\hat{\mathbf{i}}\ell\lambda_j). \quad (3.23)$$

Then using Theorem 3.2, it is easy to deduce that (cf. (3.8))

$$\left| \hbar_n \sum_{|\ell| < n} H\left(\frac{|\ell|}{n}\right) f(t^* - \ell/R) e^{\hat{\mathbf{i}}\ell x} - \sigma_n(\mu)(x) \right| \leq \alpha \mathbf{M}(t^*) (B(t^*)\Delta + 1)\Delta. \quad (3.24)$$

This leads to the following definition (cf. [4, Definition 2.3])

Definition 3.1 Let $F : \mathbb{R} \rightarrow \mathbb{C}$, $t^* \in \mathbb{R}$, $R > 0$. We define the **Signal Separation Operator SSO** by

$$\mathcal{T}_{n,R}(F)(t^*; x) = \hbar_n \sum_{|\ell| < n} H\left(\frac{|\ell|}{n}\right) f(t - \ell/R) e^{\hat{\mathbf{i}}\ell x}, \quad x \in \mathbb{R}. \quad (3.25)$$

We will use the operator to separate the components $f_j(t^*)$ and the instantaneous frequencies $\phi'_j(t^*)$ based on the noisy observations

$$F(t) = \sum_{j=1}^K f_j(t) + \epsilon(t) = \sum_{j=1}^K A_j(t) \exp(i\phi_j(t)) + \epsilon(t), \quad (3.26)$$

where for each t , $\epsilon(t)$ is a realization of a complex sub-Gaussian random variable in $\mathcal{G}(V)$. Theorem 3.1 can be translated into Theorem 3.3 below, where we abuse the notation to make the comparison easier. We note that Theorem 3.3 itself is a restatement of [4, Theorems 2.4,4.1] in a somewhat modified form taking the noise into account. In order to state this theorem, we abuse the notation in Section 3.1 again, and write (in addition to (3.18))

$$\mathbf{m}(t^*) = \min_{1 \leq \ell \leq K} |f_\ell(t^*)|, \quad \eta(t^*) = \min_{\ell \neq k} |\phi'_\ell(t^*) - \phi_k(t^*)|, \quad \eta^* = \eta(t^*)/R. \quad (3.27)$$

For brevity, we will omit the mention of t^* from our notation, unless we feel that this might cause some confusion.

Theorem 3.3 *Let $0 < \delta < 1$, $t^* \in \mathbb{R}$, $R, \Delta > 0$, and the assumptions of Theorem 3.2 be satisfied. We assume that $n = \lfloor R\Delta \rfloor$ satisfies the condition (3.11), and in addition, $n \geq 4C/\eta^*$. We assume further that*

$$\alpha \mathbf{M}(B\Delta + 1)\Delta \leq \mathbf{m}/4. \quad (3.28)$$

We define

$$\mathbb{G}(t^*) = \{x \in \mathbb{T} : |\mathcal{T}_{n,R}(F)(t^*; x)| \geq 3\mathbf{m}/4\}. \quad (3.29)$$

Then each of the following statements holds with probability exceeding $1 - \delta$.

- **(Disjoint union condition)**

The set $\mathbb{G}(t^*)$ is a disjoint union of exactly K subsets $\mathbb{G}_\ell(t^*)$,

- **(Diameter condition)**

For each $\ell = 1, \dots, K$, $\text{diam}(\mathbb{G}_\ell(t^*)) \leq 2C/n$,

- **(Separation)**

$\text{dist}(\mathbb{G}_\ell(t^*), \mathbb{G}_j(t^*)) \geq \eta/2$ for $\ell \neq j$,

- **(Interval inclusion)**

For each $\ell = 1, \dots, K$, $I_\ell = \{x \in \mathbb{T} : |x - \lambda_\ell| \leq 1/(4n)\} \subseteq \mathbb{G}_\ell(t^*)$.

Moreover, if

$$\hat{\lambda}_\ell = \arg \max_{x \in \mathbb{G}_\ell(t^*)} |\mathcal{T}_{n,R}(F)(t^*; x)|, \quad \widehat{\phi'_\ell(t^*)} = R\hat{\lambda}_\ell(\ell), \quad (3.30)$$

then

$$|\hat{\lambda}_\ell - \lambda_\ell| \leq 2C/n. \quad (3.31)$$

Remark 3.1 For the convenience of the reader, we summarize the conditions on the sampling frequency R below. We assume that for every t^* of interest,

$$R\Delta \geq \max(C_1, 4C/\eta^*) \quad (3.32)$$

and R is large enough so that with probability $> 1 - \delta$,

$$|E_n(x)| \leq C_2 V \sqrt{\frac{(\log(C_2 R \Delta)/\delta)}{R\Delta}} \quad (3.33)$$

We note that the condition (3.32) puts a lower bound on Δ , while the condition (3.28) is an upper bound on the Lipschitz constant α . In particular, the choice of Δ is a theoretically delicate one. In our experiments, this was done by experimentation. ■

Remark 3.2 In the case of a chirp

$$\phi'(t) = \begin{cases} \omega + \frac{B}{d}(t - \gamma), & \text{if } t_0 \leq t \leq t_0 + d \\ 0, & \text{otherwise,} \end{cases}$$

we have for $t^* \in [t_0, t_0 + d]$

$$|\phi'(t^* + u) - \phi'(t^*)| = \left| \frac{B}{d} \right| |u|, \quad |\phi'(t^*)| = \left| \omega + \frac{B}{d}(t^* - \gamma) \right|$$

So, we may take

$$\alpha = \frac{|B/d|}{\min_{t \in [t_0, t_0 + d]} |\omega + (B/d)(t - \gamma)|}.$$

■

4 Algorithms

In this section, we describe how the SSO can be used for signals of the form (1.4). The basic idea behind our algorithms is to apply Theorem 3.3 to different snippets of the signal. Thus, we choose a small Δ and divide the signal duration into D overlapping time intervals $I_k = [t_k - \Delta, t_k + \Delta]$, $k = 1, \dots, D$. The t_k 's are chosen such that $I_k \cap I_{k+1} \neq \emptyset$. This is to ensure that all the sampling data are considered in this experiment. Theorem 3.3 gives guidelines on how to select Δ . In practice, one has to treat this as a tunable parameter. In our experiments reported here, we chose Δ by experimentation so that it is large enough to eliminate the noise effect, but small enough to give the accurate estimation. A large value of Δ implies that there are more data points to average out the noise, but this has higher chance that the signal will start or end within the interval which leads to inaccurate estimation.

The signal restricted to I_k has the form (cf. (1.4)):

$$F_k(t) = \sum_{j=1}^{J_k} f_{j,k}(t) + \epsilon(t), \quad f_{j,k}(t) = A_{j,k}(t) \exp(\hat{\mathbf{i}}\phi_{j,k}(t)), \quad (4.1)$$

where $\epsilon(t)$ represents the noise and

$$\phi_{j,k}(t) = \omega_{j,k}(t - \gamma_{j,k}) + a_{j,k}(t - \gamma_{j,k})^2/2. \quad (4.2)$$

The SSO will be used with each F_k to obtain the parameter values for each $f_{j,k}$. In our experiments, we have focused on IFs, assuming all the amplitudes to be 1. Taken together, the set $(t_k, \widehat{\phi'_{j,k}}(t_k))$ is called the **SSO diagram**. Once we determine the IFs, the amplitudes can be determined by simply substituting the estimated IFs in SSO and more accurately by solving an appropriate least square problem. We postpone a more detailed investigation of this question to a future work.

Our methodology requires a prior knowledge of

1. a minimum separation η among all the instantaneous frequencies
2. the receiver bandwidth

$$B_{\text{rec}} \geq \max_{j,k,t} \phi'_{j,k}(t) - \min_{j,k,t} \phi'_{j,k}(t).$$

Out of these, B_{rec} is a system parameter and is always known a priori. The condition implies that all the signals are fully captured in the measurements. The minimal separation η can be found experimentally as well, and its choice will affect the performance of our algorithms. We have demonstrated this in detail in [27].

The clusters defined in Theorem 3.3 are found, using a clustering algorithm. For example, in this paper we used DBSCAN [9]. The notation we use in our algorithm is

$$([\text{scatter data}], [\text{label}]) \leftarrow \text{DBSCAN}([\text{scatter data}], [\text{neighborhood radius}], [\text{minimum number of neighbors}]). \quad (4.3)$$

Here, [scatter data] is a data matrix, and the algorithm attaches a label 1 for the cluster of interest (and -1 otherwise), based on the number of points neighboring the so called core points in a ball of radius denoted above by [neighborhood radius].

Our algorithm needs a few more tunable parameters as summarized in Table 1.

Parameters	Description
Δ	Time interval width centered at t_k , which is chosen based on Theorem 3.3
D	Number of intervals centered at t_k , which is chosen so that interval I_k 's are overlapping
D_1	Minimum number of neighbors, which can be tuned based on the number of points in the SSO diagram in the radius given by B_{rec} .
D_2	Minimum number of neighbors, which can be tuned based on the number of points in the smallest signal cluster
M	Number of partitions when signal crossover detected, which can be tuned so that some partitions contain sufficiently long linear chirps

Table 1: The tables above shows a list of tunable parameters.

Algorithm 1 is designed to find the IFs. A challenge here is to determine the correct threshold related to the unknown minimal amplitude m in the presence of noise. A value which is too small would indicate superfluous frequencies, a value which is too large would miss some frequencies. This effect is discussed in our paper [27]. There are other details such as detecting the clusters and find the right peaks which are described below. Part 2 will estimate the parameters of the instantaneous frequencies obtained by part 1 using least squares. The challenge here is to figure out where the different signal components begin and end, and which part of the signal to use in order to set up the least square problem in order to obtain reliable solutions. SSO does not work directly when there are crossover frequencies. In fact, the set up itself does not make sense in general in such cases; e.g., whether the crossover of the form X represents two linear frequencies crossing or two V -shaped frequencies touching each other. Part 3 is the refinement process where we use the facts that SSO is inherently unable to resolve crossovers and that we are dealing with linear chirps to detect the presence of such frequencies. If sufficiently long linear chirps are present on both sides of the crossover, then we can detect those using the previous two algorithms with a smaller value of Δ and interpolate to determine where the crossover happens and which chirps cross each other.

Figure 2 and 3 give flowcharts of how the algorithms are related to each other. The whole process will be illustrated step-by-step with one example in this section, and analyzed further in Section 5 with a few other examples.

j	A_j	ω_j	B_j	d_j	$t_{0,j}^*$	PRI_j	Number of pulses
1	1	1080000000	15000000	3.0e-05	1.0e-05	5.0e-05	2
2	1	1360000000	5000000	1.0e-05	1.0e-05	1.5e-05	5
3	1	1540000000	-20000000	3.0e-05	1.0e-05	0	1
4	1	1510000000	50000000	7.0e-05	1.5e-05	0	1
5	1	1480000000	-15000000	5.0e-05	3.0e-05	0	1
6	1	1040000000	-15000000	3.0e-05	1.5e-05	4.0e-05	2

Table 2: The tables above shows an example of signal ground truth parameters.

We illustrate our method using the signal with parameters as described in Table 2. In this example, we use $\epsilon(t)$ to be a Gaussian noise at -10 dB SNR. The visualizations of the raw signal $f(t)$ and its instantaneous frequency $\phi'(t)$ corresponding to the parameters in Table 2 are shown in Figure 1.

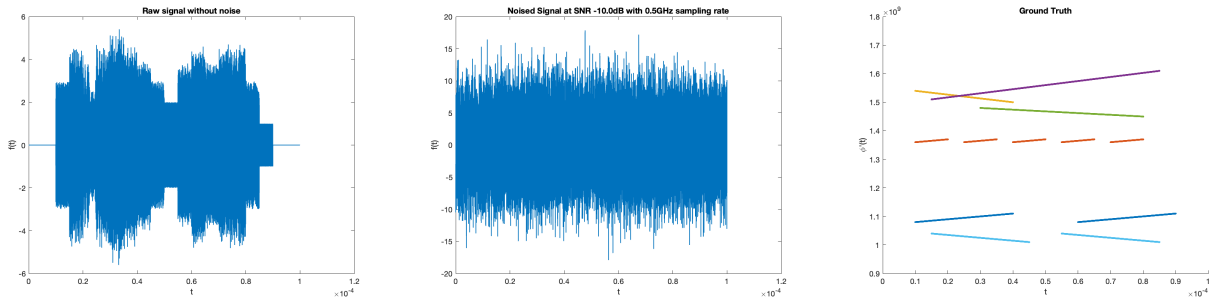


Figure 1: (Left) The raw signal $f(t)$ as given in (2.2) at sampling rate 0.5 GHz. (Middle) The noised signal $F(t) = f(t) + \epsilon(t)$ at -10 dB SNR. (Right) The ground truth of $\phi'(t)$ from (1.1).

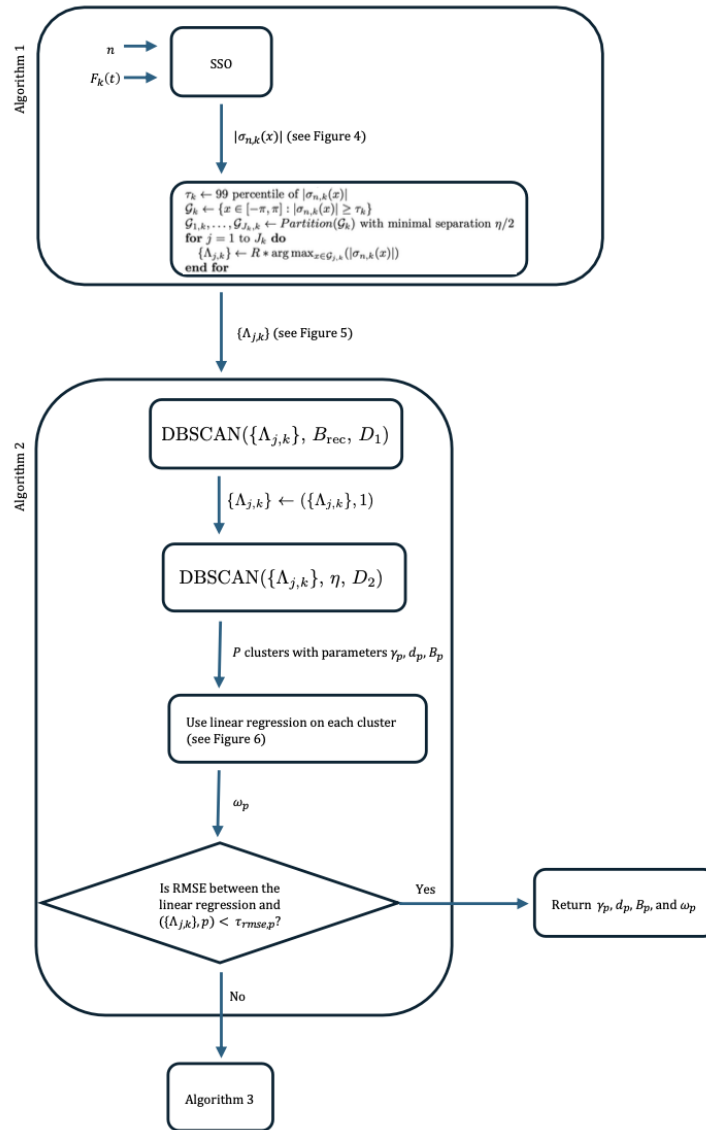


Figure 2: The flowchart diagram for our algorithm scheme.

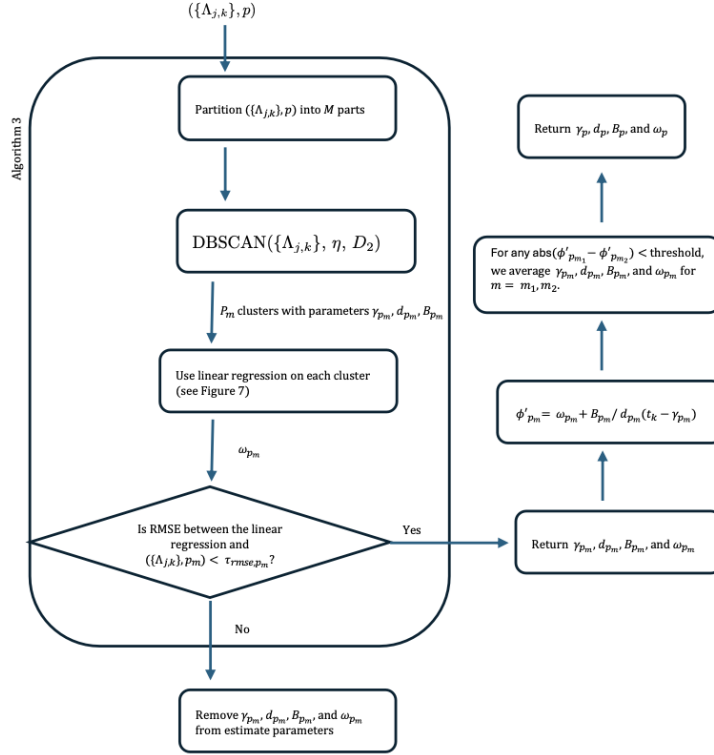


Figure 3: The flowchart diagram for our algorithm scheme.

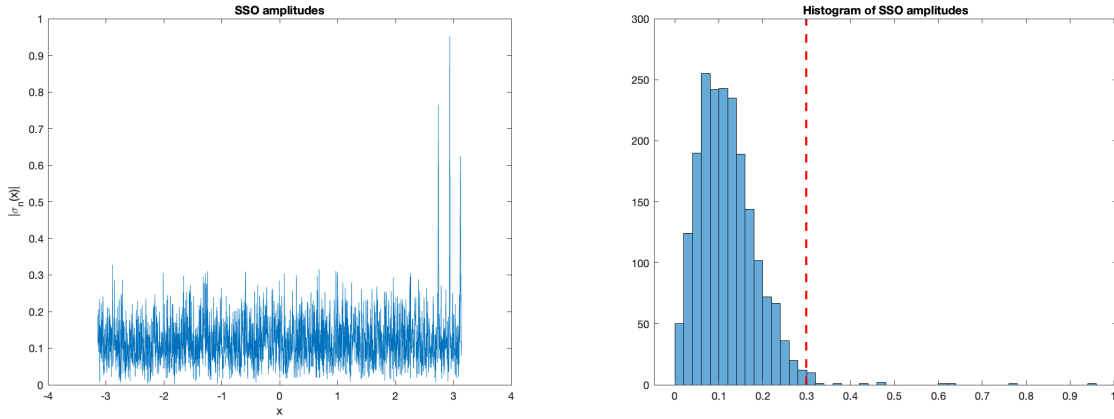


Figure 4: (Left) The raw SSO result of $F_k(t)$ at $t = 5 \times 10^{-5}$ with -10 dB SNR on 0.5 GHz sampling rate. (Right) The histogram of the SSO. The red dot line indicates the threshold $\tau_k = 99$ percentile of the SSO result.

4.1 Finding instantaneous frequencies

In this section, we describe the first stage of the algorithm illustrated in Figure 2, where we obtain the piecewise constant approximation to the the instantaneous frequencies in each snippet $F_k(t)$ for $k = 1, \dots, D$ (cf. (4.1)) using the SSO for each such snippet. The main challenge here is to determine the threshold in the definition (3.29). Since the value of the minimum amplitude \mathbf{m} is unknown, we run SSO on $F_k(t)$ and set the threshold τ_k to be 99 percentile of the power spectrum (see Figure 4). The percentile is the same for every interval I_k , but the actual value of the threshold τ_k will be different depending on the sampling frequency and the SNR.

Algorithm 1 Signal separation operator (SSO)

- a) **Input:** Minimal separation η and signal $F_k(t)$.
- b) **Output:** $\{\Lambda_{j,k}\}$
- 1: $\tilde{h}_n \leftarrow \left\{ \sum_{|\ell| < n} H\left(\frac{|\ell|}{n}\right) \right\}^{-1}$
 - 2: $\sigma_{n,k}(x) \leftarrow \tilde{h}_n \sum_{|\ell| < n} H\left(\frac{|\ell|}{n}\right) F_k(t_k - \ell/R) e^{i\ell x}$
 - 3: $\tau_k \leftarrow 99$ percentile of $|\sigma_{n,k}(x)|$
 - 4: $\mathcal{G}_k \leftarrow \{x \in [-\pi, \pi] : |\sigma_{n,k}(x)| \geq \tau_k\}$
 - 5: $\mathcal{G}_{1,k}, \dots, \mathcal{G}_{J_k,k} \leftarrow \text{Partition}(\mathcal{G}_k)$ with minimal separation $\eta/2$
 - 6: **for** $j = 1$ to J_k **do**
 - 7: $\{\Lambda_{j,k}\} \leftarrow R * \arg \max_{x \in \mathcal{G}_{j,k}} (|\sigma_{n,k}(x)|)$
 - 8: **end for**
 - 9: **Return:** $\{\Lambda_{j,k}\}$ for $j = 1, \dots, J_k$
-

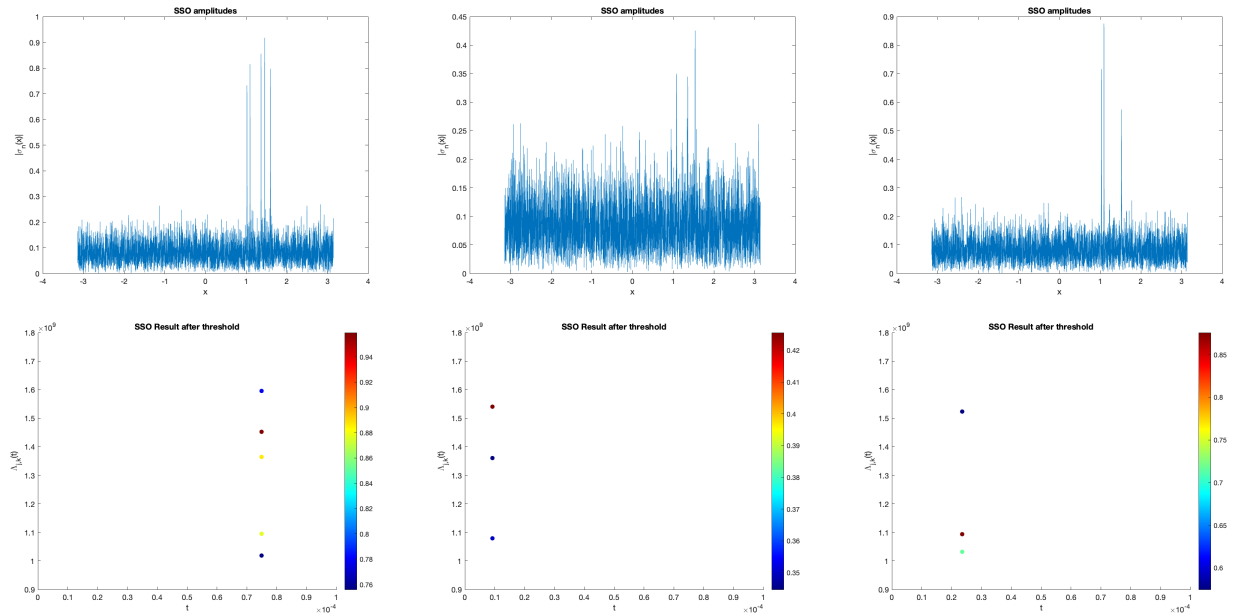


Figure 5: (Top) $|\sigma_{n,k}(x)|$ for the interval I_k . (Bottom) SSO results at t_k . (Left) The plots for $t_k = 7.5 \times 10^{-5}$ where the signals pass from the beginning through the end of the interval I_k . (Middle) The plots for $t_k = 1 \times 10^{-5}$ where the signal starts within the interval I_k . (Right) The plots for $t_k = 2.35 \times 10^{-5}$ where there are 2 signals crossover within the interval I_k .

The output of this step is the values of the instantaneous frequencies at t_k :

$$\{\Lambda_{j,k}\} = \omega_{j,k} + a_{j,k}(t_k - \gamma_{j,k}), \quad j = 1, \dots, J_k.$$

This is illustrated in Figure 5. We see that the frequencies are determined quite accurately when there is no discontinuity in the signals, and the minimal separation is large, but there is a problem when a signal starts/stops somewhere within I_k , resulting in a discontinuity or when there is a cross-over frequency, resulting in a small minimal separation.

4.2 Parameter estimation

The starting point of this step is the results of all the instantaneous frequencies in all the snippets. The resulting diagram is called the raw SSO diagram as shown in Figure 6 (Left). Knowing the receiver bandwidth B_{rec} , Algorithm 2 then concentrates on the relevant frequency part of the SSO diagram, which shows a piecewise constant approximation to the frequencies in the signal (see Figure 6 (Right)).

Algorithm 2 Parameter estimation

- a) **Input:** the receiver bandwidth B_{rec} , the minimum separation η , $\{\Lambda_{j,k}\}$ for $j = 1, \dots, J_k$, $k = 1, \dots, D$, and minimum number of neighbors D_1, D_2 .
 - b) **Output:** Estimation of ω_p, B_p, d_p and γ_p for $p = 1, \dots, P$.
 - 1: $(\{\Lambda_{j,k}\}, -1), (\{\Lambda_{j,k}\}, 1) \leftarrow \text{DBSCAN}(\{\Lambda_{j,k}\}, B_{\text{rec}}, D_1)$ to find the part of the $\{\Lambda_{j,k}\}$ relevant for our signal.
 - 2: $\{\Lambda_{j,k}\} \leftarrow (\{\Lambda_{j,k}\}, 1)$
 - 3: $(\{\Lambda_{j,k}\}, -1), (\{\Lambda_{j,k}\}, 1), \dots, (\{\Lambda_{j,k}\}, P) \leftarrow \text{DBSCAN}(\{\Lambda_{j,k}\}, \eta, D_2)$ to separate the $\{\Lambda_{j,k}\}$ into P clusters.
 - 4: **for** $p = 1$ to P **do**
 - 5: $\Gamma_p \leftarrow [(t_k, y_{j,k}) \text{ for } y_{j,k} \in (\{\Lambda_{j,k}\}, p)]$
 - 6: $\gamma_p \leftarrow \min(t_k)$ for $(t_k, y_{j,k}) \in \Gamma_p$.
 - 7: $d_p \leftarrow \max(t_k) - \min(t_k)$ for $(t_k, y_{j,k}) \in \Gamma_p$
 - 8: $B_p \leftarrow (\max(y_{j,k}) - \min(y_{j,k}))/2$ for $(t_k, y_{j,k}) \in \Gamma_p$
 - 9: Use linear regression on 50% of Γ_p that has highest $|\sigma_{n,k}(x)|$ to obtain the parameter estimation for ω_p .
 - 10: $\tau_{\text{rmse},p} \leftarrow 1\%$ of mean $(y_{j,k})$ for $(t_k, y_{j,k}) \in \Gamma_p$.
 - 11: **if** RMSE_p defined in (4.4) $> \tau_{\text{rmse},p}$ **then**
 - 12: Perform Algorithm 3
 - 13: **end if**
 - 14: **end for**
 - 15: **Return:** ω_p, B_p, d_p and γ_p for $j = 1, \dots, P$.
-

Given the minimum separation, we can separate these approximations for different signal components using DBSCAN. Algorithm 2 then focuses on this approximation in each component of the signal, and finds the corresponding parameters using linear regression. The result of this operation is shown in Figure 7.

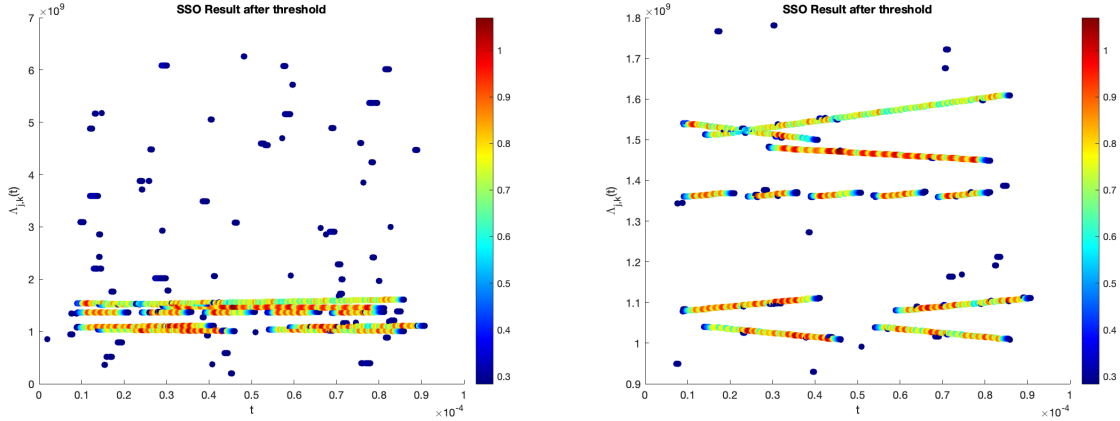


Figure 6: (Left) The plot of threshold SSO result $\{\Lambda_{j,k}\}$ for $j = 1, \dots, J_k$, $k = 1, \dots, D$ by choosing $\Delta = 2 \times 10^{-6}$, $D = 2500$, $D_1 = D/2$, $D_2 = D/100$, and t_k are equidistant samples from 0 to 1×10^{-4} . (Right) The plot of threshold SSO result after step 1 of Algorithm 2.

4.3 Refinements

Algorithm 3 focuses on working on the clusters in the SSO diagram where the signals crossover; i.e. the distance between two or more signals is less than the minimum separation η .

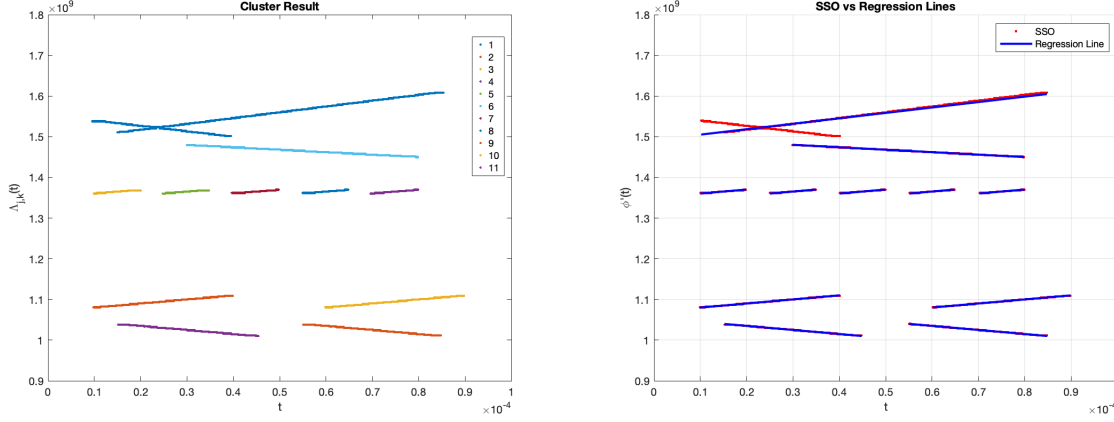


Figure 7: (Left) The plot of signal components after using DBSCAN. (Right) The comparison plot between the SSO result vs the regression lines of $((\{\Lambda_{j,k}\}, 1), p)$. This is the result of Algorithm 2 without performing Algorithm 3; i.e. skipping steps 8 - 10 of Algorithm 2.

Algorithm 3 Handling signals crossover

- a) **Input:** the minimum separation η , $(\{\Lambda_{j,k}\}, p)$ for p when signals crossover, and minimum number of neighbors D_2 , partition number M .
 - b) **Output:** Estimation of ω_p, B_p, d_p and γ_p for p when signals crossover.
 - 1: $\{\Lambda_{j,k}\} \leftarrow (\{\Lambda_{j,k}\}, p)$
 - 2: partitions \leftarrow partition $\{\Lambda_{j,k}\}$ into M parts.
 - 3: **for** partition m in partitions **do**
 - 4: $(\{\Lambda_{j,k}\}, -1), (\{\Lambda_{j,k}\}, 1), \dots, (\{\Lambda_{j,k}\}, P_m) \leftarrow \text{DBSCAN}(\{\Lambda_{j,k}\}, \eta, D_2)$ to separate the $\{\Lambda_{j,k}\}$ into P_m clusters.
 - 5: **for** $p_m = 1$ to P_m **do**
 - 6: $\Gamma_{p_m} \leftarrow [(t_k, y_{j,k}) \text{ for } y_{j,k} \in (\{\Lambda_{j,k}\}, p_m)]$
 - 7: $\gamma_{p_m} \leftarrow \min(t_k)$ for $(t_k, y_{j,k}) \in \Gamma_{p_m}$.
 - 8: $d_{p_m} \leftarrow \max(t_k) - \min(t_k)$ for $(t_k, y_{j,k}) \in \Gamma_{p_m}$
 - 9: $B_{p_m} \leftarrow (\max(y_{j,k}) - \min(y_{j,k}))/2$ for $(t_k, y_{j,k}) \in \Gamma_{p_m}$
 - 10: Use linear regression on 50% of Γ_{p_m} that has highest $|\sigma_{n,k}(x)|$ to obtain the parameter estimation for ω_{p_m} .
 - 11: $\tau_{\text{rmse}, p_m} \leftarrow 1\%$ of $\text{mean}(y_{j,k})$ for $(t_k, y_{j,k}) \in \Gamma_{p_m}$.
 - 12: **if** RMSE_{p_m} defined in (4.4) $> \tau_{\text{rmse}, p_m}$ **then**
 - 13: Remove $\omega_{p_m}, B_{p_m}, d_{p_m}$, and γ_{p_m} from estimate parameters and return fail to detect this part of the signal.
 - 14: **end if**
 - 15: **end for**
 - 16: **end for**
 - 17: Compute ϕ'_{p_m} for each partition. If any two or more of the ϕ'_{p_m} 's are within 10% each other, then average them and update these parameters to ω_p, B_p, d_p and t_p .
 - 18: **Return:** ω_p, B_p, d_p , and γ_p for p when signals crossover.
-

The part where signals crossover is detected by computing the RMSE between $y_{j,k}$ for $(t_k, y_{j,k}) \in \Gamma_p$ and the regression line using the formula

$$\text{residue}_{j,k,p} = |y_{j,k} - (\omega_p + B_p/d_p(t_k - \gamma_p))|, \quad (4.4)$$

$$\text{RMSE}_p = \sqrt{\frac{1}{D} \sum_{k=1}^D \sum_{j=1}^{J_k} \text{residue}_{j,k,p}^2}. \quad (4.5)$$

If the RMSE_p is larger than a small threshold, we then proceed to the refinement algorithm, Algorithm 3.

To refine this part of the signal, we partition the signal into small intervals as shown in Figure 8. Finally, we

set a threshold on the $\phi'_{p_m}(t)$ and connect them if the differences between two or more $\phi'_{p_m}(t)$'s are within the threshold. The final result is shown in Figure 9.

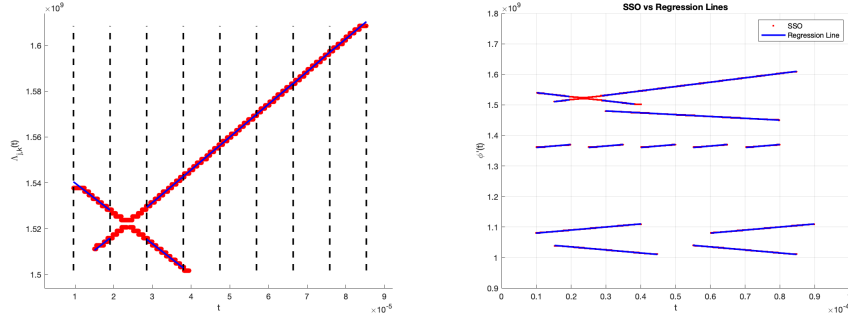


Figure 8: (Left) The plot of crossing signals after performing step 1 - 13 of the Algorithm 3 by choosing $M = 8$ partitions. (Right) The comparison plot between the SSO result vs the regression lines of $\{\Lambda_{j,k}\}$ after performing step 1 - 13 of the Algorithm 3.

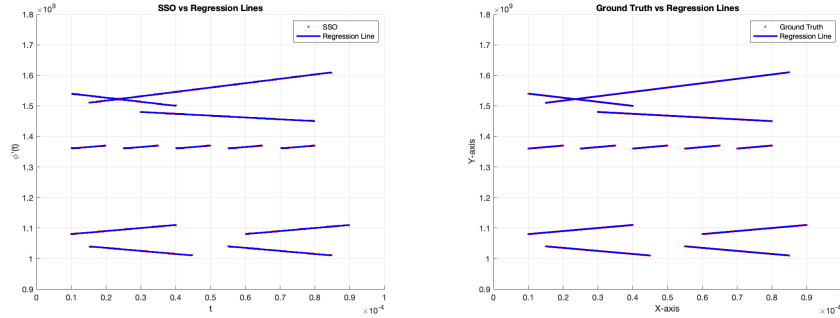


Figure 9: The final comparison plot between the SSO result vs the regression lines of $\{\Lambda_{j,k}\}$ (left) and the ground truth vs the regression lines (right).

5 Numerical experiments

5.1 Data generation

In order to test our methodology, we generated a dataset of 7 examples, each consisting of 6 signals, which will be made available at a web location after the paper is published.

We add noise to our generated original signal using the formula

$$\mathbf{F} = \mathbf{f} + \boldsymbol{\epsilon}, \quad (5.1)$$

where \mathbf{F} is a matrix of the noised signal $F(t)$, \mathbf{f} is a matrix of the original signal $f(t)$, \mathbf{n} is a matrix of Gaussian noise, and $\boldsymbol{\epsilon}$ is a matrix of the noise $\epsilon(t)$ defined by

$$\boldsymbol{\epsilon} = \frac{\|\mathbf{f}\|_2}{10^{\text{SNR}/20} * \|\mathbf{n}\|_2} * \mathbf{n}. \quad (5.2)$$

5.2 Numerical results

To assess the robustness and performance of the proposed Signal Separation Operator (SSO) method, we conducted a series of controlled numerical experiments across a variety of scenarios. These experiments were designed to evaluate the impact of key signal characteristics, including minimal frequency separation, SNR, sampling rate, and the presence of frequency crossovers.

The details for all the experiments are listed in Tables 3 and 4 in the Appendix.

5.2.1 Minimal separation

The algorithm demonstrates strong performance when signal components are sufficiently separated in frequency. As illustrated in Figure 10, the method accurately recovers the instantaneous frequencies and associated parameters in both non-intersecting and cleanly intersecting cases. However, performance degrades in scenarios where the minimal separation between components becomes too small. In such cases, the spectral peaks associated with different components may become indistinct, leading to inaccurate clustering and parameter estimation. This limitation is primarily due to the inherent resolution bounds imposed by the kernel size and the sampling interval.

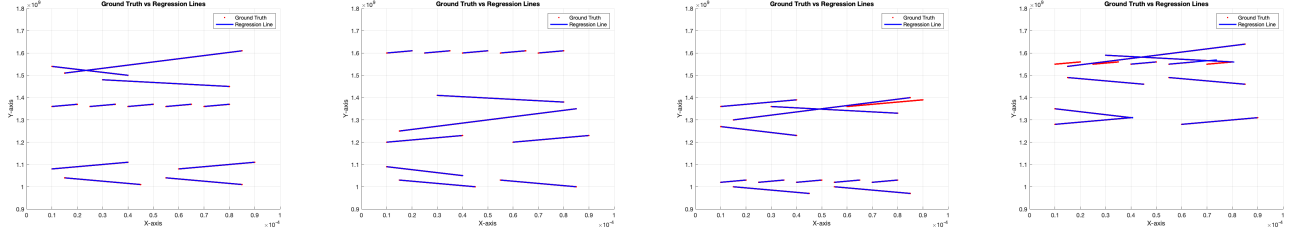


Figure 10: Ground truth vs regression result plots for example 1, 2, 3, and 4 with SNR -10 dB and sampling rate 0.5 GHz. Our algorithm works well in case of no crossover and clear crossover signals, but does not work so well when the minimum separation among signals is low.

5.2.2 Robustness to noise

The method remains effective even under high noise conditions. To illustrate, we compute the the root mean square error (RMSE) in each experiment by

$$\text{RMSE} = \text{mean} \left(\sqrt{\frac{1}{D} \sum_{k=1}^D \sum_{j=1}^{J_k} \left(\frac{\phi'_{j,k}(t_k) - \widehat{\phi'_{j,k}}(t_k)}{\phi'_{j,k}(t_k)} \right)^2} \right). \quad (5.3)$$

In our experiments, we took the mean over 16 trials for each choice of the signal, the sampling rate, and SNR. As shown in Figure 11, the root mean square error (RMSE) remains low for SNR levels ranging from 10 dB to -30 dB. The algorithm maintains RMSE values within acceptable bounds, provided that the sampling rate is sufficient. The combination of localized kernel averaging and peak detection in the frequency domain allows the method to suppress noise effectively.

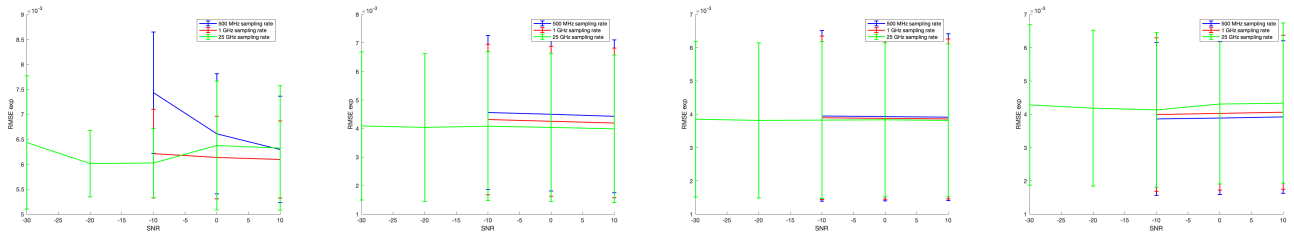


Figure 11: The sampling rate performance plots of vary SNR vs RMSE for example 1, 2, 3, and 4. The RMSE was comparing between the ground truth and the estimation parameters of $\phi(t)$ in (1.1).

5.2.3 Sampling Rate

Sampling rate plays a critical role in frequency resolution and noise resilience. As shown in Figure 12, increasing the sampling rate from 0.5 GHz to 25 GHz significantly improves the accuracy of instantaneous frequency estimation, particularly in cases with minimal separation or closely spaced crossovers. In this figure, a heat map is used to visualize the estimation error computed in equation (4.4), where the color indicates the magnitude of error. This color-coded representation helps to clearly highlight the improvement in performance with higher sampling rates.

Higher sampling rates yield a finer time grid, which enhances the operator’s ability to resolve subtle frequency variations and distinguish between overlapping components.

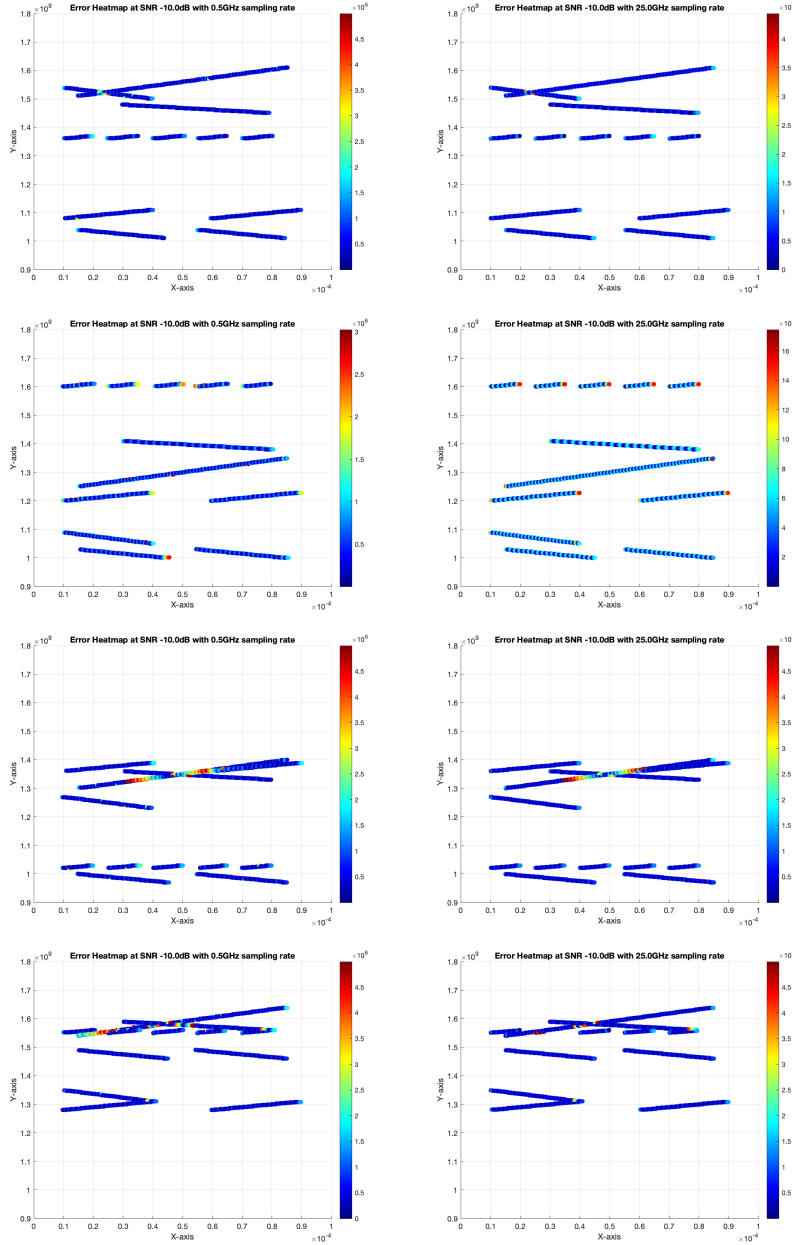


Figure 12: Heat map of the errors for example 1, 2, 3, and 4 with SNR -10 dB at sampling rate 0.5 GHz (left) vs sampling rate 25 GHz (right). One may notice that the higher sampling rate examples can deal with the smaller minimal separation among signals better.

5.2.4 Comparison with SST

We recall that the most often used method for finding IF’s is EMD, which is purely heuristic. The method known as synchrosqueezing transform method (SST) is based on a solid mathematical foundation, and works better than EMD. In this section we compare our results with those obtained by using SST. As mentioned earlier, there are many versions of SST. We use the implementation of the SST algorithm as described in Section III of [36]. Figure 13 shows that our implementation of this algorithm works for certain signals at high SNR levels and deteriorates at lower levels. We observed that the maximum frequency that the SST method can take is 0.2 GHz at sampling rate

0.5 GHz while our dataset has maximum frequency at 1.6 GHz. Figure 14 illustrates that the SST fails to work in the regime in which we are interested in this paper.

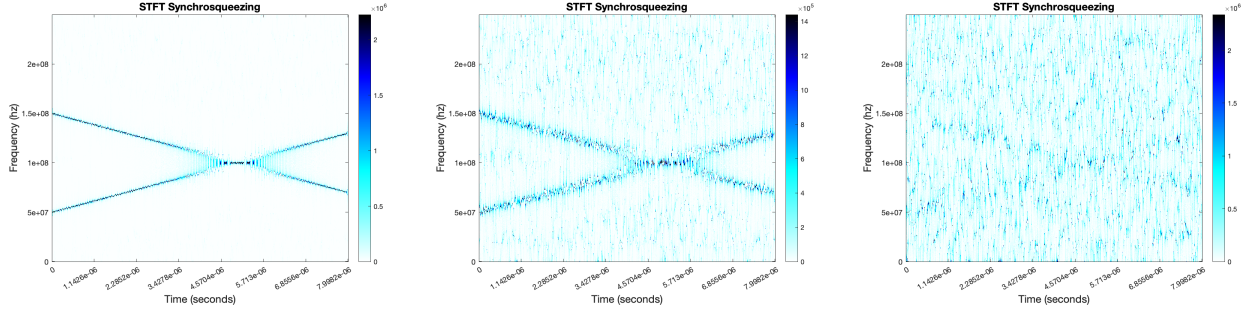


Figure 13: The examples of SST plot with sampling rate 0.5 GHz at SNR 20 dB (left), SNR 0 dB (middle), and SNR -10 dB (right) for signals $f(t) = e^{2\pi i(15 \times 10^7 t - 5 \times 10^{12} t^2)} + e^{2\pi i(5 \times 10^7 t + 5 \times 10^{12} t^2)}$.

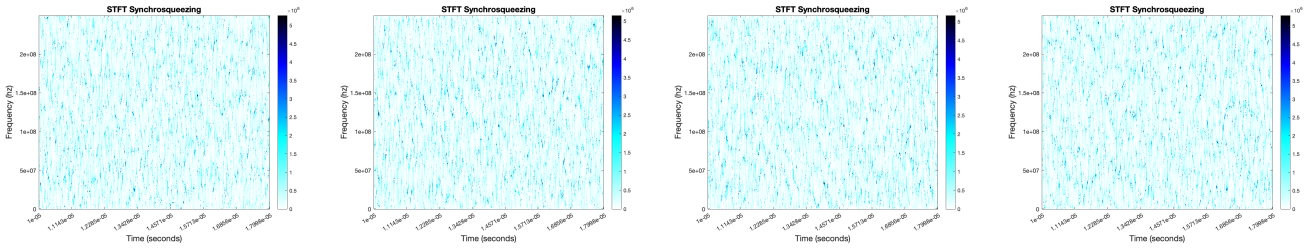


Figure 14: The SST plots for example 1, 2, 3, and 4 with SNR 0 dB and sampling rate 0.5 GHz.

6 Conclusions

Separation of a superposition of blind source signals is an important problem in audio and radar signal processing with many applications, including electronic warfare and electronic intelligence. In this paper, we have modified a method proposed in [4] for solving this problem in the case when the instantaneous frequencies of the components are linear. The method is based on a filtered FFT, and hence, is very fast. While the paper [4] assumes the frequencies to be slowly and continuously varying, our modification includes the case when the signals are discontinuous and when there are crossover frequencies present. We analyze theoretically the behavior of SSO in the presence of noise, giving insight into the relationship between the sampling frequency, desired accuracy, and noise. We have illustrated the effectiveness our method with a few well chosen examples, and tested it on a small database of 7 signals, demonstrating a consistent behavior. Our method outperforms the SST algorithm given in [36].

7 Appendix

We report the statistics for 16 trials for each of the SNR and sampling rates for each signal, where the RMSE is computed using (5.3).

SNR (dB)	Example label	Sampling rate (GHz)	Total signals	Detected signals	RMSE	Standard Deviation
10	1	0.500000	12	12	0.006295	0.001066
10	1	1.000000	12	12	0.006095	0.000770
10	1	25.000000	12	12	0.006325	0.001249
0	1	0.500000	12	12	0.006610	0.001203
0	1	1.000000	12	12	0.006133	0.000828
0	1	25.000000	12	12	0.006375	0.001291
-10	1	0.500000	12	12	0.007433	0.001214
-10	1	1.000000	12	12	0.006211	0.000888
-10	1	25.000000	12	12	0.006022	0.000690
-20	1	25.000000	12	12	0.006012	0.000666
-30	1	25.000000	12	12	0.006436	0.001336
10	2	0.500000	12	12	0.004428	0.002676
10	2	1.000000	12	12	0.004197	0.002619
10	2	25.000000	12	12	0.003990	0.002588
0	2	0.500000	12	12	0.004496	0.002685
0	2	1.000000	12	12	0.004255	0.002624
0	2	25.000000	12	12	0.004038	0.002593
-10	2	0.500000	12	12	0.004565	0.002698
-10	2	1.000000	12	12	0.004315	0.002633
-10	2	25.000000	12	12	0.004086	0.002607
-20	2	25.000000	12	12	0.004038	0.002590
-30	2	25.000000	12	12	0.004088	0.002597
10	3	0.500000	12	11	0.003915	0.002504
10	3	1.000000	12	11	0.003859	0.002402
10	3	25.000000	12	11	0.003818	0.002293
0	3	0.500000	12	12	0.003934	0.002532
0	3	1.000000	12	11	0.003877	0.002427
0	3	25.000000	12	11	0.003834	0.002314
-10	3	0.500000	12	11	0.003950	0.002561
-10	3	1.000000	12	11	0.003895	0.002452
-10	3	25.000000	12	11	0.003825	0.002355
-20	3	25.000000	12	11	0.003814	0.002332
-30	3	25.000000	12	11	0.003850	0.002335
10	4	0.500000	12	9	0.003918	0.002293
10	4	1.000000	12	9	0.004061	0.002310
10	4	25.000000	12	10	0.004335	0.002404
0	4	0.500000	12	9	0.003886	0.002292
0	4	1.000000	12	9	0.004025	0.002306
0	4	25.000000	12	10	0.004310	0.002406
-10	4	0.500000	12	9	0.003861	0.002296
-10	4	1.000000	12	9	0.003994	0.002305
-10	4	25.000000	12	10	0.004132	0.002319
-20	4	25.000000	12	10	0.004184	0.002339
-30	4	25.000000	12	10	0.004283	0.002408

Table 3: The tables above shows full performances of our algorithm.

SNR (dB)	Example label	Sampling rate (GHz)	Total signals	Detected signals	RMSE	Standard Deviation
10	5	0.500000	12	12	0.005752	0.002110
10	5	1.000000	12	12	0.005199	0.002565
10	5	25.000000	12	12	0.004693	0.002723
0	5	0.500000	12	12	0.005926	0.001830
0	5	1.000000	12	12	0.005325	0.002474
0	5	25.000000	12	12	0.004781	0.002699
-10	5	0.500000	12	10	0.006114	0.001440
-10	5	1.000000	12	12	0.005460	0.002364
-10	5	25.000000	12	12	0.004971	0.002684
-20	5	25.000000	12	12	0.004873	0.002693
-30	5	25.000000	12	12	0.004874	0.002666
10	6	0.500000	12	10	0.004385	0.002373
10	6	1.000000	12	10	0.004349	0.002319
10	6	25.000000	12	10	0.004416	0.002305
0	6	0.500000	12	10	0.004383	0.002387
0	6	1.000000	12	9	0.004365	0.002332
0	6	25.000000	12	10	0.004406	0.002313
-10	6	0.500000	12	10	0.004380	0.002400
-10	6	1.000000	12	9	0.004380	0.002345
-10	6	25.000000	12	10	0.004337	0.002298
-20	6	25.000000	12	10	0.004344	0.002290
-30	6	25.000000	12	8	0.004395	0.002322
10	7	0.500000	12	10	0.004440	0.002269
10	7	1.000000	12	10	0.004427	0.002231
10	7	25.000000	12	11	0.004435	0.002193
0	7	0.500000	12	9	0.004436	0.002280
0	7	1.000000	12	10	0.004441	0.002241
0	7	25.000000	12	11	0.004436	0.002204
-10	7	0.500000	12	9	0.004435	0.002290
-10	7	1.000000	12	9	0.004453	0.002252
-10	7	25.000000	12	10	0.004409	0.002211
-20	7	25.000000	12	11	0.004409	0.002202
-30	7	25.000000	12	9	0.004441	0.002214

Table 4: The tables above shows full performances of our algorithm.

References

- [1] Stéphane Boucheron, Gábor Lugosi, and Pascal Massart. *Concentration inequalities: A nonasymptotic theory of independence*. Oxford university press, 2013.
- [2] Hou Changbo, Hua Lijie, Liu Guowei, and Lin Yun. Radar signal separation and recognition based on semantic segmentation. In *2020 7th International Conference on Dependable Systems and Their Applications (DSA)*, pages 385–390, 2020.
- [3] Wang Chao, Sun Liting, Liu Zhangmeng, and Huang Zhitao. A radar signal deinterleaving method based on semantic segmentation with neural network. *IEEE Transactions on Signal Processing*, 70:5806–5821, 2022.
- [4] Charles K Chui and H. N. Mhaskar. Signal decomposition and analysis via extraction of frequencies. *Applied and Computational Harmonic Analysis*, 40(1):97–136, 2016.
- [5] I. Daubechies, J. Lu, and H. T. Wu. Synchrosqueezed wavelet transforms: an empirical mode decomposition-like tool. *Applied and computational harmonic analysis*, 30(2):243–261, 2011.
- [6] I. Daubechies and S. Maes. A nonlinear squeezing of the continuous wavelet transform based on auditory nerve models. *Wavelets in medicine and biology*, pages 527–546, 1996.

- [7] Baron Gaspard Riche De Prony. Essai expérimental et analytique: sur les lois de la dilatabilité de fluides élastique et sur celles de la force expansive de la vapeur de l'alcool, a différentes températures. *Journal de l'école polytechnique*, 1(22):24–76, 1795.
- [8] Rashi Dutt, Anuradha Baloria, Ram Chandra Prasad V., Radhakrishna ESMP, and Amit Acharyya. Discrete wavelet transform based unsupervised underdetermined blind source separation methodology for radar pulse deinterleaving using antenna scan pattern. *IET Radar, Sonar and Navigation*, 13(8):1350–1358, 2019.
- [9] Martin Ester, Hans-Peter Kriegel, Jörg Sander, Xiaowei Xu, et al. A density-based algorithm for discovering clusters in large spatial databases with noise. In *kdd*, volume 96, pages 226–231, 1996.
- [10] F. Filbir, H. N. Mhaskar, and J Prestin. On the problem of parameter estimation in exponential sums. *Constructive Approximation*, 35(3):323–343, 2012.
- [11] Simone Filice, Danilo Croce, and Roberto Basili. A robust machine learning approach for signal separation and classification. In João M. Sanches, Luisa Micó, and Jaime S. Cardoso, editors, *Pattern Recognition and Image Analysis*, pages 749–757, Berlin, Heidelberg, 2013. Springer Berlin Heidelberg.
- [12] Rafael G. Licursi de Mello and Fernando Rangel de Sousa. Precise techniques to detect superimposed radar pulses on esm systems. *IET Radar, Sonar and Navigation*, 12(7):735–741, 2018.
- [13] D. Gabor. Theory of communication. part 1: The analysis of information. *Journal of the Institution of Electrical Engineers-Part III: Radio and Communication Engineering*, 93(26):429–441, 1946.
- [14] Wang Gongming, Chen Shiwen, Hu Xueruobai, and Yuan Junjian. Radar emitter sorting and recognition based on time-frequency image union feature. In *2019 IEEE 4th International Conference on Signal and Image Processing (ICSIP)*, pages 165–170, 2019.
- [15] N. E. Huang, Z. Shen, S. R. Long, M. C. Wu, H. H. Shih, Q. Zheng, N.C. Yen, C. C. Tung, and H. H. Liu. The empirical mode decomposition and the Hilbert spectrum for nonlinear and non-stationary time series analysis. *Proceedings of the Royal Society of London. Series A: Mathematical, Physical and Engineering Sciences*, 454(1971):903–995, 1998.
- [16] Li Jiang, Lin Li, and Guo qing Zhao. Pulse-compression radar signal sorting using the blind source separation algorithms. In *2015 International Conference on Estimation, Detection and Information Fusion (ICEDIF)*, pages 268–271, 2015.
- [17] Hongbin Jin, Weilin Luo, Hao Li, and Lingyan Dai. Underdetermined blind source separation of radar signals based on genetic annealing algorithm. *The Journal of Engineering*, 2022(3):261–273, 2022.
- [18] Shashank S. Joshil, Cuong M. Nguyen, V. Chandrasekar, J. Christine Chiu, and Yann Blanchard. Separating cloud and drizzle signals in radar doppler spectra using a parametric time domain method. *Journal of Atmospheric and Oceanic Technology*, 37(9):1669 – 1680, 2020.
- [19] Jordan Juliano, Jaron Lin, Alex Erdogan, and Kiran George. Radar pulse on pulse identification parallel fft and power envelope algorithm. In *2020 11th IEEE Annual Ubiquitous Computing, Electronics and Mobile Communication Conference (UEMCON)*, pages 0609–0613, 2020.
- [20] Janne Lehtomäki. *Analysis of energy based signal detection*. University of Oulu, 2005.
- [21] Lin Li, Ningning Han, Qingtang Jiang, and Charles K Chui. A chirplet transform-based mode retrieval method for multicomponent signals with crossover instantaneous frequencies. *Digital Signal Processing*, 120:103262, 2022.
- [22] Jaron Lin, Jordan Juliano, Alex Erdogan, and Kiran George. Pulse separation using independent component analysis. In *2020 11th IEEE Annual Ubiquitous Computing, Electronics and Mobile Communication Conference (UEMCON)*, pages 0946–0950, 2020.
- [23] Yanchao Liu and Qunying Zhang. Improved method for deinterleaving radar signals and estimating pri values. *IET Radar, Sonar and Navigation*, 12(5):506–514, 2018.

- [24] Yongjian Liu, Peng Xiao, Hongchao Wu, and Weihua Xiao. Lpi radar signal detection based on radial integration of choi-williams time-frequency image. *Journal of Systems Engineering and Electronics*, 26(5):973–981, 2015.
- [25] Shoji Makino. *Audio source separation*, volume 433. Springer, 2018.
- [26] H. N. Mhaskar and J. Prestin. On local smoothness classes of periodic functions. *Journal of Fourier Analysis and Applications*, 11(3):353–373, 2005.
- [27] HN Mhaskar, S Kitimoon, and Raghu G Raj. Robust and tractable multidimensional exponential analysis. *arXiv preprint arXiv:2404.11004*, 2024.
- [28] Aditya Arie Nugraha, Antoine Liutkus, and Emmanuel Vincent. Multichannel audio source separation with deep neural networks. *IEEE/ACM Transactions on Audio, Speech, and Language Processing*, 24(9):1652–1664, 2016.
- [29] Mustafa Atahan Nuhoglu, Yasar Kemal Alp, Mehmet Ege Can Ulusoy, and Hakan Ali Cirpan. Image segmentation for radar signal deinterleaving using deep learning. *IEEE Transactions on Aerospace and Electronic Systems*, 59(1):541–554, 2023.
- [30] Philip Pace. 2008.
- [31] Lihui Pang, Yilong Tang, Qingyi Tan, Yulang Liu, and Bin Yang. A mle-based blind signal separation method for time–frequency overlapped signal using neural network. *EURASIP Journal on Advances in Signal Processing*, 2022(1):121, 2022.
- [32] Xujun Peng, Zhiyu Shi, Pengfei Jin, Xiaoyan Zhang, Zheng Yang, and Xuelei Feng. A blind source separation method: Nonlinear chirp component analysis. *Mechanical Systems and Signal Processing*, 216:111491, 2024.
- [33] Zhiyu Shao, Jiangheng He, and Shunshan Feng. Separation of multicomponent chirp signals using morphological component analysis and fractional fourier transform. *IEEE Geoscience and Remote Sensing Letters*, 17(8):1343–1347, 2020.
- [34] Jia Su, Mengru Xi, Yanyun Gong, Mingliang Tao, Yifei Fan, and Ling Wang. Time-varying wideband interference mitigation for sar via time-frequency-pulse joint decomposition algorithm. *IEEE Transactions on Geoscience and Remote Sensing*, 60:1–16, 2022.
- [35] Ewa Swiercz, Krzysztof Konopko, and Dariusz Janczak. Time-chirp distribution for detection and estimation of lpi radar signals. In *2020 21st International Radar Symposium (IRS)*, pages 362–367, 2020.
- [36] Gaurav Thakur, Eugene Brevdo, Neven S Fuckar, and Hau-Tieng Wu. The synchrosqueezing algorithm for time-varying spectral analysis: Robustness properties and new paleoclimate applications. *Signal processing*, 93(5):1079–1094, 2013.
- [37] Longhao Xie, Wenxing Ren, Ziyang Cheng, Ming Li, and Huiyong Li. Power and waveform resource allocation method of lpi netted radar for target search and tracking. *IET Radar, Sonar and Navigation*, 19(1):e70022, 2025.
- [38] Yi Yuan, Xubo Liu, Haohe Liu, Mark D Plumbley, and Wenwu Wang. Flowsep: Language-queried sound separation with rectified flow matching. In *ICASSP 2025-2025 IEEE International Conference on Acoustics, Speech and Signal Processing (ICASSP)*, pages 1–5. IEEE, 2025.
- [39] Peng Zhou, Yang Yang, Shiqian Chen, Zhike Peng, Khandaker Noman, and Wenming Zhang. Parameterized model based blind intrinsic chirp source separation. *Digital Signal Processing*, 83:73–82, 2018.